Molecular Crystals and Liquid Crystals
Publication details, including instructions for authors and subscription information:
http://www.tandfonline.com/loi/gmcl20

Detecting Exoplanets with a Liquid-Crystal-Based Vortex Coronagraph

Eugene Serabyn [a] & Dimitri Mawet [b]

[a] Jet Propulsion Laboratory, California Institute of Technology, Pasadena, CA, 91109, USA

[b] European Southern Observatory, Alonso de Córdova 3107, Vitacura, 7630355, Santiago, Chile

Version of record first published: 11 May 2012.

To cite this article: Eugene Serabyn & Dimitri Mawet (2012): Detecting Exoplanets with a Liquid-Crystal-Based Vortex Coronagraph, Molecular Crystals and Liquid Crystals, 559:1, 69-75

To link to this article: http://dx.doi.org/10.1080/15421406.2012.658683

Mol. Cryst. Liq. Cryst., Vol. 559: pp. 69–75, 2012

ISSN: 1542-1406 print/1563-5287 online
DOI: 10.1080/15421406.2012.658683

Taylor & Francis
Taylor & Francis Group

Detecting Exoplanets with a Liquid-Crystal-Based Vortex Coronagraph

EUGENE SERABYN[1,*] AND DIMITRI MAWET[2]

[1]Jet Propulsion Laboratory, California Institute of Technology, Pasadena, CA 91109, USA
[2]European Southern Observatory, Alonso de Córdova 3107, Vitacura 7630355, Santiago, Chile

Planets beyond our own solar system are difficult to image directly because of their proximity to significantly brighter stars. In order to suppress the intense starlight, a high-performance optical coronagraph is required, and the optical vortex coronagraph can in theory enable observations very close to stars. The vortex phase masks needed to implement this approach have been manufactured as circularly symmetric half-wave plates made of liquid crystal polymers, and initial on-sky tests have been carried out. This approach has in fact already allowed the successful detection of exoplanets as close as two diffraction beam widths from a bright star, at contrasts of approximately 10^{-5}. Significantly improved performance should be possible in the near future.

Keywords Coronagraphy; exoplanets; vortex

Introduction

The direct imaging of the faint planets around nearby stars ("exoplanets") is becoming increasingly feasible due to new observational techniques and image calibration approaches. As a result, imaging surveys of nearby stars have recently succeeded in uncovering the first several directly imaged exoplanets [1–5]. However, the exoplanets detected to date are mostly exceptionally bright "tip of the iceberg" cases, while the ultimate goal of imaging terrestrial analogs requires contrasts of $\sim 10^{-10}$. Extending imaging observations to more typical planets and a wider variety of stars thus calls for large improvements in small-angle high-contrast observational capabilities. In particular, with reflected starlight proportional to the inverse square of the star-planet separation (Fig. 1), it is important to be able to observe as close to stars as possible. This is especially important in the space-based case, for which telescope sizes are constrained by cost.

To enable very high-contrast observations near bright stars, it is necessary to minimize both scattered and diffracted starlight. The former implies the need for nearly perfectly flat wavefronts, and hence for actively-corrected optical systems. The latter implies an optical system capable of removing the bright stellar contribution, which is the goal of stellar "coronagraphs", named in analogy to the solar coronagraphs long used to study the environment of our own Sun [6]. One of the coronagraphs closest to the ideal case is

*Address correspondence to Eugene Serabyn, Jet Propulsion Laboratory, California Institute of Technology, Pasadena, CA 91109, USA. Tel.: 818-393-5243; Fax: 818-393-4357. E-mail: gene.serabyn@jpl.nasa.gov

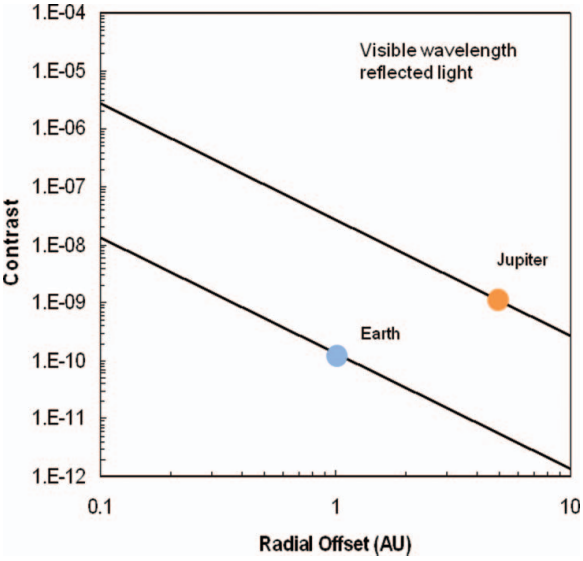

Figure 1. Visible-wavelength flux ratio (contrast) of earth-like and Jupiter-like planets around a solar-type G2 star, as a function of the star-planet separation in astronomical units (1.5×10^{11} m).

the optical vortex coronagraph [7–10], which is theoretically capable of observing faint companions to within about one diffraction beam width (i.e., $\approx 1\ \lambda/D$, where λ is the observation wavelength and D is the telescope diameter) of host stars. Liquid crystals have played a key role in the development of the optical vortex coronagraph [11,12], and so this paper briefly describes the operation of the optical vortex coronagraph, before turning to progress in the development of liquid-crystal-based vortex phase masks.

The Optical Vortex Coronagraph

Astronomical imaging relies on large-aperture telescopes that collect and focus the approximately plane waves arriving from very distant stars. With actively-corrected imaging, the stellar image consists of a focal-plane diffraction-limited point spread function (PSF) that is described by the classical Airy pattern in the ideal case (i.e., for a clear telescope aperture with no obstruction due to an on-axis secondary mirror). However, in general the bright stellar PSF completely swamps the much dimmer off-axis PSFs due to any nearby exoplanets. Therefore, a coronagraphic reimaging stage is inserted prior to the detector plane with the goal of improving the planet/star flux ratio (i.e., the contrast).

Two steps are involved in the implementation of an optical vortex coronagraph (Fig. 2). First, the stellar PSF is centered on a focal-plane vortex phase mask. The phase mask applies an azimuthal phase ramp to the PSF that wraps to an even multiple of 2π in a circuit about the center. As any planets present would be off-axis, their light would bypass the center of the vortex, and be relatively unaffected by passage through a localized off-axis region of the focal plane phase mask. After passage through the vortex mask, the light is recollimated with a lens or mirror, generating a downstream pupil image. In this pupil image, due to the action of the vortex mask, the starlight and the planet light arrive spatially separated, with the starlight outside the image of the input pupil, and the planet light still inside it, as described further below. The second step is thus simply to block the starlight in this pupil

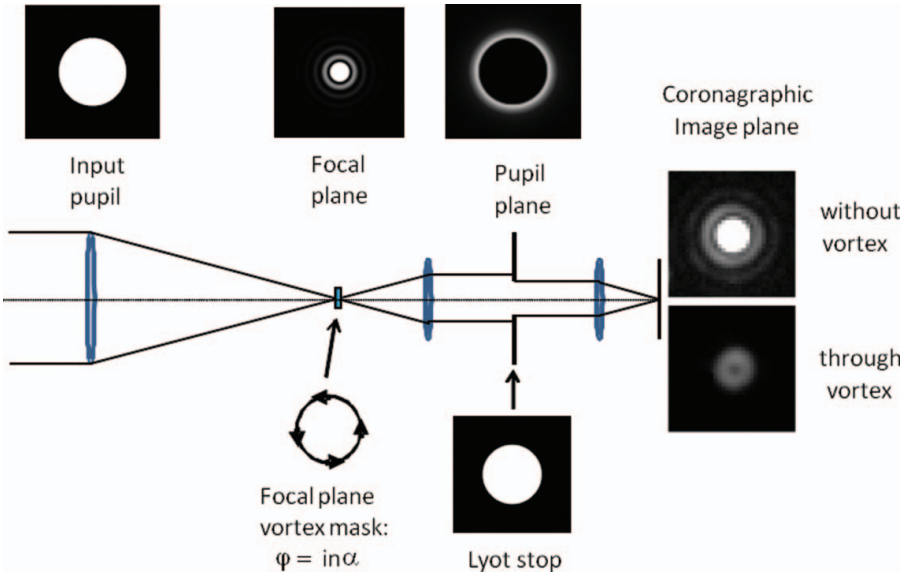

Figure 2. The layout of the optical vortex coronagraph. The stellar PSF is centered on a focal-plane vortex mask, redirecting the starlight beyond the subsequent pupil image, where it is blocked by an opaque stop.

plane with an opaque (Lyot) stop, while letting the planet light pass through the center of the stop. The operation of the vortex coronagraph is now described in further detail.

A clear telescope input pupil can be described by a field distribution, $P_i(r)$, of

$$P_i(r) = \begin{cases} 1 & \text{for } r < A \\ 0 & \text{for } r > A, \end{cases} \tag{1}$$

where r is the radial coordinate, and A is the radius of the input aperture. Focusing the light leads, via a Fourier transform, to the usual focal-plane field distribution,

$$E_f(\theta) \propto \frac{J_1(kA\theta)}{kA\theta}, \tag{2}$$

where J_1 is the Bessel function of order 1, k is the wavenumber, and θ is the angular radial offset from the center of the stellar PSF. In the normal (i.e., non-coronagraphic) imaging case, the generation of a downstream pupil via a second Fourier transform (lens) would yield an output pupil given, after some mathematical manipulation, by

$$P_o(r) \propto \int_0^\infty J_o(kr\theta) J_1(kA\theta) d\theta, \tag{3}$$

Using [13]

$$\int_0^\infty J_n(at) J_{n-1}(bt) dt = \begin{cases} 0 & \text{for } a < b \\ \frac{b^{n-1}}{a^n} & \text{for } a > b, \end{cases} \tag{4}$$

in this simple case then leads to a constant flux for $r < A$, i.e., inside the original pupil. Thus in this case, the original pupil is restored,

$$P_o(r) = P_i(r), \tag{5}$$

as expected.

On the other hand, applying a vortex phase shift of order 2 to the focal plane field of Eqn. (2) yields

$$E_f(\theta) \propto \quad e^{i2\alpha} \frac{J_1(kA\theta)}{kA\theta}, \tag{6}$$

where α is the azimuthal coordinate. Reimaging the pupil with a post-vortex lens (i.e., performing a Fourier transform) as before, in this case leads instead to an output pupil of

$$P_o(r) \propto \quad e^{i2\alpha} \int_0^\infty J_2(kr\theta) J_1(kA\theta) d\theta \tag{7}$$

Equation (4) then yields instead (including proper normalizations)

$$E(r) = \begin{cases} 0 & \text{for} \quad r < A \\ -\left(\dfrac{A}{r}\right) e^{2i\alpha} & \text{for} \quad r > A \end{cases}. \tag{8}$$

In this case, all of the starlight appears outside of the original pupil! Thus, the seemingly innocuous change in the kernel of the integral has led to the starlight being moved perfectly from the interior to the exterior of the geometric image of the pupil. The starlight can then be rejected quite simply by blocking the region exterior to the image of the telescope pupil with an opaque stop (termed the "Lyot" stop). On the other hand, the light from any off-axis planets, having bypassed the center of the vortex phase plate, reaches the Lyot plane with its original distribution, i.e., the planet light remains interior to the pupil. It thus propagates without significant attenuation to the detector plane, yielding a significantly improved contrast relative to the star. Note that the vortex mask thus serves merely as a means of redirecting the starlight. The starlight is actually removed by the subsequent Lyot stop.

Vortex Phase Masks

Of course, in order to make use of this starlight rejection approach, the manufacture of the requisite vortex phase masks must be feasible. The needed azimuthal phase ramp can in principle be provided by a dielectric with a spiral thickness distribution (the scalar vortex [8]), or by passage through a rotationally symmetric half-wave plate (the vector vortex [7]). The vector vortex approach has already yielded very promising results, as is now described.

However, the use of a vortex phase mask at a focus, instead of in an extended beam, introduces a very stringent requirement. In particular, in the focused case the stellar light is concentrated into a very small diffraction spot at the center of the vortex. The geometrical phase structure of the vortex phase plate must thus be accurately maintained in to very small radii, i.e., the axial singularity must thus be very well-defined, so that the starlight cannot "leak" through any central irregularity, or "disorientation region" in the phase pattern. The central region must at a minimum be small compared to Fλ, where F is the beam

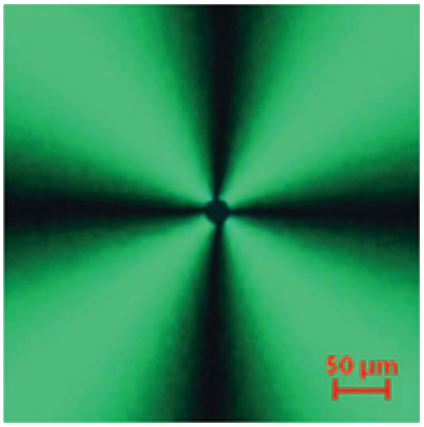

Figure 3. An infrared ($\lambda = 2.16$ μm) vortex phase mask manufactured by JDS Uniphase, shown between crossed polarizers [12]. This mask has a roughly 25 μm central disorientation region that is covered with a 25 μm Al circular spot.

focal ratio and λ is the wavelength. For typical optical focal ratios of a few tens, and a wavelength of $\sim$0.5 μm, this implies that central confusion regions need to be significantly smaller than $\sim$10 μm. Ideally, any central imperfection in the vortex phase mask should be reduced to sub-wavelength scales, or $<$0.5 μm for optical wavelengths. However, for longer near-infrared wavelengths (1–2.5 μm), where most ground-based adaptive optics systems provide good performance, these conditions on the central disorientation region are more relaxed by a factor of a few.

Alternatively, a small residual central disorientation region can be masked off with a small central opaque mask, leaving a more or less perfect vortex structure outside of a central opaque region. However, such an opaque obstruction would introduce other diffraction issues, such as leakage near the edge of the pupil, as in the case of the classical opaque Lyot coronagraph [6], and so this solution is less optimal than reducing the disorientation region sufficiently. Nevertheless, a central blocker can be used to optimize performance in early generation masks with extended central disorientation regions.

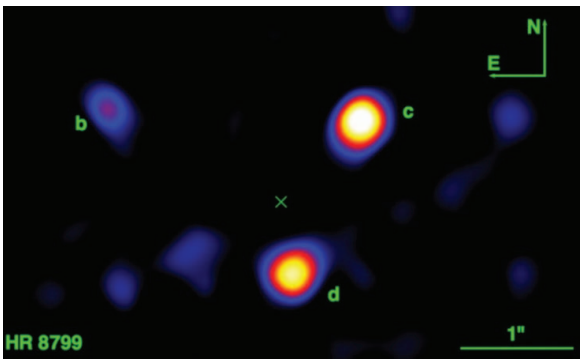

Figure 4. An infrared image [14] of three exoplanets in HR8799 acquired with a vector vortex coronagraph at the Palomar Observatory.

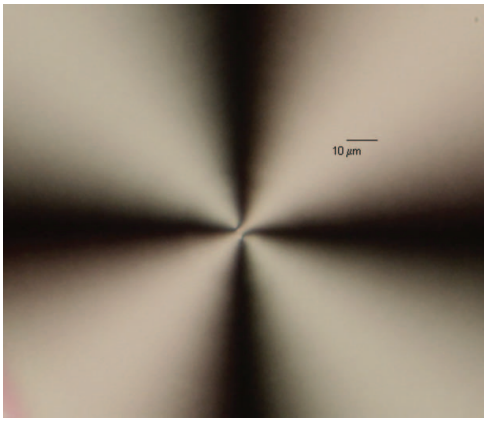

Figure 5. An optical-wavelength vortex phase mask recently manufactured by Beam Engineering shown between crossed polarizers [15].

In practice, central disorientation regions of ∼25 microns [12] have been achieved in vector vortex masks aimed at near-infrared wavelengths that were manufactured for JPL by JDS Uniphase (Fig. 3). The size of the residual disorientation region in this case was limited by mechanical tolerances in the rotation stages involved in the manufacturing process [11], but as these masks were aimed at the ground-based infrared case, a central disorientation region of the size achieved is indeed somewhat smaller than Fλ (35 μm), and so meets the first requirement. With these masks, a 25 μm central blocker was added to reduce the effect of the central disorientation region as described. In fact, these infrared vortex masks have provided sufficient starlight rejection to have recently allowed the detection of three exoplanets around the nearby star HR8799 [14] using a fairly small (1.5 m) telescope aperture (Fig. 4). As one of these planets lies at an angle of roughly 2λ/D from the star for an aperture of the size (1.5 m) used, these observations provide a very good demonstration of the potential of the vortex coronagraph for small angle observations close to bright stars.

More recently, even smaller disorientation regions, ≤5 μm across (Fig. 5), have been achieved by Beam Co. on masks aimed at optical wavelengths (for space-based usage), using newly developed optical manufacturing techniques. The new steps include the use of different materials, the equalization of the illumination pattern in the manufacturing stage, and the "printing" of higher order vortices from lower order vortices [15]. Nevertheless, further work will be necessary in order to reduce the central disorientation region to sub-wavelength scales. Additional work is also needed to ensure broadband performance, in order to enable the deep broadband rejection of starlight. Nevertheless, fundamental limits have not yet been reached, allowing a great deal of room for further progress.

Acknowledgment

This work was carried out at the Jet Propulsion Laboratory, California Institute of Technology, under contract with the National Aeronautics and Space Administration.

References

[1] Kalas, P. *et al.*, (2008). *Science*, *322*, 1345.
[2] Marois, C. *et al.*, (2008). *Science*, *322*, 1348.

[3] Marois, C. *et al.*, (2010). *Nature*, *468*, 1080.
[4] Lagrange, A.-M. *et al.*, (2009). *Astron. & Astrophys. Lett.*, *493*, L21.
[5] Lagrange, A-M. *et al.*, (2010). *Science*, *329*, 57.
[6] Lyot, B. (1939). *Mon. Not. R. Astron. Soc.*, *99*, 580.
[7] Mawet, D., Riaud, P., Absil, O., & Surdej, J. (2005). *Astrophys. J.*, *633*, 1191.
[8] Foo, G., Palacios, D. M., & Swartzlander, G. A., Jr. (2005). *Optics Letters*, *30*, 3308.
[9] Swartzlander, G. (2009). *J. Opt. A.*, *11*, 1464.
[10] Guyon, O., Pluzhnik, E. A., Kuchner, M. J., Collins, B., & Ridgway, S. T. (2006). *Astrophys. J. Suppl.*, *167*, 81.
[11] Mawet, D. *et al.*, (2009). *Optics Express*, *17*, 1902.
[12] Mawet, D., Serabyn, E., Stapelfeldt, K., & Crepp, J. (2009). *Astrophys. J. Lett.*, *702*, L47.
[13] Abramowitz, M., & Stegun, I. A. (1972). *Handbook of Mathematical Functions, National Bureau of Standards*, Applied Mathematics Series 55, p. 487.
[14] Serabyn, E., Mawet, D., & Burruss, R. (2010). *Nature*, *464*, 1018.
[15] Tabiryan, N. *et al.*, (2012). in Proceedings of 2012 IEEE Aerospace Conf., Big Sky, Montana, p. 1.